Winter 2-2013

Mechanical Behavior of a Magnesium Alloy Nanocomposite under Conditions of Static Tension and Dynamic Fatigue

T. S. Srivatsan
University of Akron, Main Campus

C. Godbole
University of Akron, Main Campus

T. Quick
University of Akron, main campus

M. Paramsothy

M. Gupta

JMEPEG (2013) 22:439–453
DOI: 10.1007/s11665-012-0276-2

1059-9495/$19.00

Mechanical Behavior of a Magnesium Alloy Nanocomposite Under Conditions of Static Tension and Dynamic Fatigue

T.S. Srivatsan, C. Godbole, T. Quick, M. Paramsothy, and M. Gupta

(Submitted February 29, 2012; in revised form May 23, 2012; published online July 13, 2012)

In this paper, the intrinsic influence of nano-alumina particulate (Al_2O_{3p}) reinforcements on microstructure, microhardness, tensile properties, tensile fracture, cyclic stress-controlled fatigue, and final fracture behavior of a magnesium alloy is presented and discussed. The unreinforced magnesium alloy (AZ31) and the reinforced composite counterpart (AZ31/1.5 vol.% Al_2O_3) were manufactured by solidification processing followed by hot extrusion. The elastic modulus, yield strength, and tensile strength of the nanoparticle-reinforced magnesium alloy were noticeably higher than the unreinforced counterpart. The ductility, quantified by elongation-to-failure, of the composite was observably lower than the unreinforced monolithic counterpart (AZ31). The nanoparticle-reinforced composite revealed improved cyclic fatigue resistance over the entire range of maximum stress at both the tested load ratios. Under conditions of fully reversed loading ($R = -1$) both materials showed observable degradation in behavior quantified in terms of cyclic fatigue life. The conjoint influence of reinforcement, processing, intrinsic microstructural features and loading condition on final fracture behavior is presented and discussed.

Keywords aluminum oxide, cyclic fatigue life, fracture, hardness, magnesium alloy, metal-matrix composite, microstructure, particulate reinforcement, tensile response

1. Introduction

Since their initial emergence as a viable material for structural applications continued research efforts have enabled the family of metal-matrix composites (MMCs) for selection and use in a spectrum of performance-critical and even non-performance-critical applications. This has been made possible due essentially to their improved mechanical properties to include a high specific modulus (E/ρ), high strength-to-weight ratio (σ/ρ), improved material damping capacity, increased wear resistance coupled with decreased thermal expansion when compared one-on-one with the monolithic counterpart. The metal magnesium has a low density of 1.73 g/cm^3, which is approximately two-thirds of that of aluminum (ρ = 2.77 g/cm^3), one-fourth that of zinc (ρ = 6.88 g/cm^3), and one-fifth that of steel (ρ = 7.88 g/cm^3), which enables it to offer high specific strength (σ/ρ) in comparison with the contending conventional alloys. This noteworthy property coupled with its affinity, by way of compatibility, with the reinforcing phases, be it ceramic or metallic, has provided both an incentive and stimulus for initiating scientific and technology relevant research studies on magnesium alloy-based MMCs as a subject of intense research (Ref 1-4).

Magnesium alloys based on the Mg-Al-Zn ternary system have been the focus for comprehensive research studies since the early 1980s. These research studies aimed at investigating the use and viability of magnesium alloy-based MMCs for applications in the industries of automobile, aerospace, and even ground transportation systems. Cost-effective processing and precious selection of the reinforcing phase that has compatibility with the metal matrix coupled with an innate ability to enhance properties of the resultant composite has been the focus of recent research studies (Ref 1, 4). Trojanova et al. (Ref 5) manufactured magnesium alloy (AZ91) composite reinforced with δ-Al_2O_3 (Saffil®) short fibers using the squeeze cast technique and subsequently investigated its deformation response under conditions of compressive loading. Morisada et al. (Ref 6) independently studied the effect of silicon carbide particulates (SiCp) on microstructural development and hardness of magnesium alloy (AZ31)-based composite manufactured using friction stir processing. Wang et al. (Ref 7) reported an observable improvement in tensile strength of magnesium alloy AZ91D that was reinforced with particulates of titanium carbide (TiCp) when deformed at elevated temperatures. Ho et al. (Ref 8) studied the intrinsic influence of copper particulates and reported an: (a) improvement in stiffness, 0.2% yield strength and ultimate tensile strength, and (b) a marginal reduction in ductility. In another independent study around the same time period, Habibnejad-Korayem et al. (Ref 9) manufactured the composite based on magnesium alloy (AZ31) reinforced with alumina (Al_2O_3) using the stir casting method and reported noticeable improvements in both hardness

T.S. Srivatsan and **C. Godbole**, Division of Materials Science and Engineering, Department of Mechanical Engineering, The University of Akron, Akron, OH 443250-3903; **T. Quick**, Department of Geology, The University of Akron, Akron, OH 443250-3903; and **M. Paramsothy** and **M. Gupta**, Department of Mechanical Engineering, National University of Singapore, 9, Engineering Drive 1, Singapore 117-576, Singapore. Contact e-mail: tsrivatsan@uakron.edu.

and tensile properties (Ref 9). Nguyen and Gupta (Ref 10) investigated the intrinsic influence of alumina particulates (Al_2O_{3p}) on both failure strain and work of fracture of solidification processed magnesium alloy AZ31B and reported a transition in fracture mode from predominantly brittle to shear-type ductile failure. Paramsothy et al. (Ref 11) used the spray deposition-based solidification processing technique to successfully integrate alumina (Al_2O_3) nanoparticles in magnesium alloy AZ31. They were able to synthesize a hybrid magnesium alloy (AZ31/AZ91) reinforced with nano-sized particles of (i) aluminum oxide or alumina (Al_2O_3) (Ref 12), and (ii) silicon nitride (Si_3N_4) (Ref 13). They reported their synthesized composite material to have improved tensile strength and improved compressive strength when compared one-on-one with the monolithic counterpart.

In more recent years, researchers have devoted their attention towards developing light weight magnesium-based MMCs that offer improved resistance to cyclic deformation to overcome several of the inadequacies shown by the monolithic counterpart for selection and use in performance demanding applications. Thus, an understanding of the fatigue life, crack propagation kinetics, and intrinsic mechanisms and microscopic mechanisms governing the overall fatigue performance of these novel magnesium composites has gained increasing importance and significance (Ref 14, 15). Srivatsan et al. (Ref 16) studied the quasi-static and cyclic fatigue behavior of magnesium alloy (Z6) discontinuously reinforced with SiC particulates (SiCp) over a range of stress amplitudes and at different test temperatures. Around the same time Vaidya and Lewandowski (Ref 17) evaluated the influence of changes in both the size and volume fraction of the reinforcing particle (SiCp) on high cycle fatigue behavior of magnesium alloy (AZ91D) composite. Much effort been made to study the behavior of magnesium alloy AZ91 reinforced with alumina fibers. Llorca et al. (Ref 18), in their independent study reported an increase in both yield strength and elastic modulus by the use of alumina particulate reinforcements along with a concurrent improvement in cyclic fatigue strength with an increase in volume fraction of the reinforcing alumina fibers. Ochi et al. (Ref 19) made an attempt to investigate the effect of volume fraction of alumina short fibers on high cycle fatigue properties of magnesium alloy AZ91D alloy. They reported the reinforcement to be effective in increasing fatigue strength of the composite with crack initiation occurring at the clusters of short alumina fibers. In their independent study, Riehemann et al. (Ref 20) investigated the influence of reinforcement on a magnesium alloy-based composite subjected to thermal cycles and measured the strain amplitude-dependent damping.

An examination of the available literature reveals an absence of research related to investigating, understanding and rationalizing the stress-controlled high cycle fatigue behavior of nanoparticulate-reinforced magnesium alloy. In the present study, an attempt has been made to evaluate, understand and rationalize the mutually interactive influences of processing and nano-sized alumina particulate (Al_2O_3p) reinforcements on quasi-static tension, stress amplitude-controlled high cycle fatigue (HCF) and resultant fracture behavior of magnesium alloy AZ31. The fracture surfaces of the fully deformed and failed test specimens were examined in a scanning electron microscope (SEM) with the primary objective of understanding and establishing the microscopic mechanisms governing deformation. The monolithic alloy and the alumina particulate-reinforced nanocomposite were prepared by the technique of disintegrated melt deposition (DMD) followed by hot extrusion (Ref 21-25).

2. Materials and Processing

2.1 Material

The magnesium alloy (AZ31) and the alumina particulate-reinforced composite (AZ31 + 1.5 vol.% Al_2O_3) used in this research study were provided as extruded rods having a diameter of 8 mm and an overall length of 300 mm by National University of Singapore (NUS: Singapore). The nominal chemical composition of AZ31 magnesium alloy was: 2.50-3.50 wt.% Al, 0.60-1.40 wt.% Zn, 0.15-0.40 wt.% Mn, 0.10 wt.% Si, 0.05 wt.% Cu, 0.01 wt.% Fe, 0.01 wt.% Ni, balance Mg. The magnesium alloy AZ31 (used as matrix for the composite) was provided by Tokyo Magnesium Co. Ltd (Yokohama, Japan) to the National University of Singapore in the form of ingots. These ingots were then sectioned into smaller blocks and precision machined to remove the layer of oxide or scales on the surface. The alumina particles (Al_2O_3) having a size of 50 nm were used as reinforcement for the magnesium alloy to engineer the magnesium alloy-based MMC. The reinforcing Al_2O_3 particles were procured from Baikowski (Japan).

2.2 Processing

2.2.1 Magnesium Alloy AZ31. DMD (Ref 21-25) was used to cast the monolithic AZ31 alloy. The process involved heating blocks of alloy AZ31 to 750 °C. The heating was carried out using resistance heating on a graphite crucible (having an arrangement for pouring at the bottom) with argon gas as the inert atmosphere. To ensure a near-uniform distribution of heat, the melt was stirred for 5 min at 460 rpm using a 45° pitch twin blade mild steel impeller. To avoid and/or minimize interactions between the melt and the mild steel impeller, the impeller was coated with Zirtex 25 (86% ZrO_2, 8.8% Y_2O_3, 3.6% SiO_2, 1.2% K_2O and Na_2O with 0.3% trace of the inorganic). The molten melt was then released through a 10-mm diameter orifice located at the base of the crucible. At a distance of 265 mm from the pouring point the melt was disintegrated using two jets of argon gas (at the rate of 25 L per minute) oriented normal to the melt stream. The disintegrated melt slurry was then deposited onto a metallic substrate located 500 mm from the disintegration point. An ingot having a diameter of 40 mm was obtained following the deposition stage.

2.2.2 The Nanoparticle Composite (AZ31 + 1.5 vol.% Al_2O_3). To form the nanocomposite reinforced with 1.5 vol.% alumina (aluminum oxide (Al_2O_3)) fine powder of the reinforcing alumina was wrapped in an aluminum foil having minimal weight (<0.50 wt.%) with respect to magnesium alloy (AZ31). All of the other parameters related to the technique of DMD were essentially unchanged to that used for the monolithic alloy.

Billets of both the monolithic alloy and the nanoparticle-reinforced composite were precision machined to a size of 35 mm diameter and subsequently hot extruded on a 150-ton hydraulic press at an extrusion ratio of 20.25:1. The extrusion was carried out at 350 °C. The billets were held at 400 °C for a

full sixty minutes in a furnace prior to extrusion. Colloidal graphite was used as the lubricant during extrusion. The rods obtained following extrusion measured 8 mm in diameter.

3. Experimental Procedures

3.1 Sample Preparation

The extruded rods of the monolithic AZ31 alloy and alumina particle-reinforced composite (diameter = 8 mm and length = 300 mm) were precision machined to obtain cylindrical specimens with threaded ends for both the uniaxial tension and stress-controlled high cycle fatigue testing. The machining was carried out in conformance with specifications outlined in Standard E-8 of American Society for Testing Materials Standard (ASTM). The major stress axis was taken to be along extrusion direction of the rod stock. The overall length of the specimen measured 2.3 inch (58 mm) with a diameter of 0.25 inch (6.3 mm) at the thread section and diameter of 0.125 inch (3 mm) at the gage section. The gage length measured 0.5 inch (12.5 mm).

3.2 Microstructural Characterization

To understand the specific influence of processing on (i) grain size and shape and (ii) size, shape, and distribution of the second-phase particles in the monolithic alloy (AZ31) and the effect of nano-alumina (Al_2O_3) particulate reinforcements on intrinsic microstructural changes in the nanocomposite, initial microstructural characterization of the as-provided extruded rod was carried out. No attempt was made in this study to determine the size of the reinforcing Al_2O_3 particulates. The as-provided extruded rod of AZ31 alloy and AZ31/1.5 vol.% Al_2O_3 composite were prepared for examination in a light optical microscope (Model: Mitutoyo FS70) and photographed using standard bright field illumination technique. Test samples were cut perpendicular to the direction of extrusion and mounted in bakelite. The mounted samples were prepared for optical microscopy observation using standard metallography preparation techniques. Coarse polishing was performed using progressively finer grades (320-grit, 400-grit, and 600-grit) of silicon carbide (SiC) impregnated emery paper. Finish polishing to near mirror-like finish was accomplished using 1-μm alumina powder suspended in distilled water as the lubricant. The polished samples were then etched using acetic-picral, i.e., a solution mixture of 5 mL acetic acid, 6 g picric acid, 10 mL water, and 100 mL ethanol. The fine polished surface of the test specimen was then carefully immersed in the etchant till such time a brown film formed and immediately rinsed in running water followed by drying using a hot air gun.

3.3 Mechanical Testing

Hardness measurements were performed on polished surfaces of both the monolithic and composite samples on plane perpendicular to the direction of extrusion. Each reading was an average of at least four separate measurements taken at random places on the surface of the polished specimens. The test was performed on a Vickers microhardness tester (Model: Tukon 2100) using a load of 200 g and a dwell time of 15 s.

Uniaxial tension tests and stress-controlled high cycle fatigue Tests were performed on a fully automated, close-loop servohydraulic mechanical test machine (Model: INSTRON: 8500 Plus) in laboratory environment (Relative Humidity of 55 pct) at room temperature (25 °C). The servohydraulic machine was equipped with a 22 kip (100 kN) load cell and the tensile tests were performed at a constant strain rate of 0.0001 per second using a 15.5 mm gage length clip-on extensometer that was mounted on the gage section of the test specimen. A PC-based Data Acquisition Software (DAS) was used to record both the stress and strain measurements during the monotonic tension test.

The stress amplitude-controlled high cycle fatigue tests were performed on both the monolithic alloy (AZ31) and the composite (AZ 31/Al_2O_3) using a sinusoidal waveform and at stress ratios [R = minimum stress/maximum stress] of 0.1 and −1.0. The tests were conducted at a constant frequency of 5 Hz with the prime objective of establishing the variation of maximum stress ($\sigma_{maximum}$) on cyclic fatigue life (N_f). The maximum stress was taken to be a fraction of the yield stress of the candidate material as obtained from the uniaxial tension test. The number of cycles to cause complete failure or separation is taken as the fatigue life (N_f).

3.4 Failure-Damage Analysis

A high magnification SEM (Model: FEI Quanta 200) was used to examine the fracture surfaces of the deformed and failed

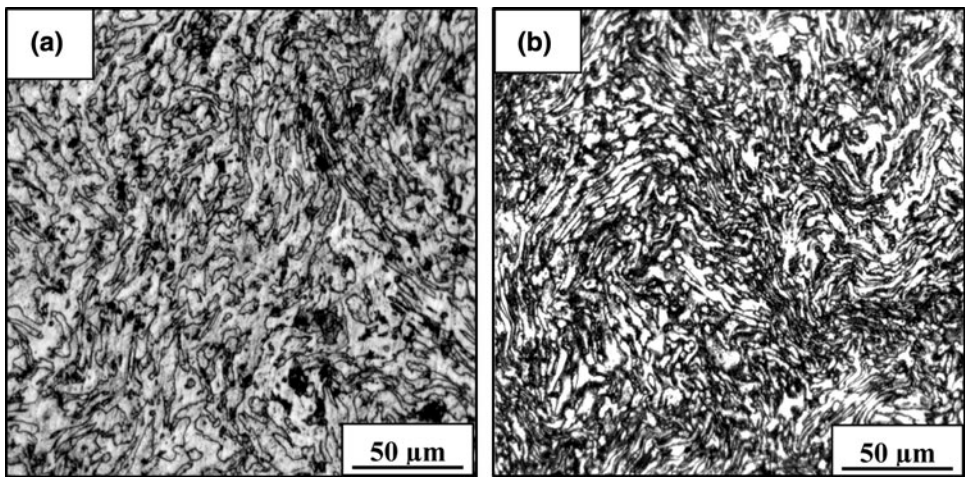

Fig. 1 Optical microstructures (a) AZ31 and (b) AZ31/1.5 vol.% Al_2O_3

Table 1 Microhardness measurements of monolithic AZ31 and alumina-reinforced composite

Material		Trail 1	Trail 2	Trail 3	Trail 4	Average hardness, kg/mm^2	Average hardness, GPa
AZ31	D1, mm	75.3	74.6	80.8	71.7	…	…
	D2, mm	73.3	76.8	84.4	72.8	…	…
	Hv, kg/mm^2	67.0	65.0	54.0	69.0	63.8	0.625
AZ31/1.5 vol.% Al_2O_3	D1, mm	64.2	64.3	66.6	62.7	…	…
	D2, mm	64.5	63.9	64.6	62.5	…	…
	Hv, kg/mm^2	90	90	86	95	90.25	0.884

Load 200 g, dwell time 15 s

Table 2 Mechanical properties of AZ31 and AZ31/1.5 vol.% Al_2O_3 deformed under uniaxial tension at room temperature

Specimen	Elastic modulus		Yield strength		Ultimate tensile strength		Elongation GL = 0.5″, %	Reduction in area, %	Tensile ductility $\ln(A_o/A_r)$, %
	ksi	GPa	ksi	MPa	ksi	MPa			
AZ31	6567	45	29.6	204	42.6	294.0	13.5	20.4	22.8
AZ31/1.5 vol.% Al_2O_3	7054	49	33.1	228	43.9	303.0	10.5	18.3	20.2

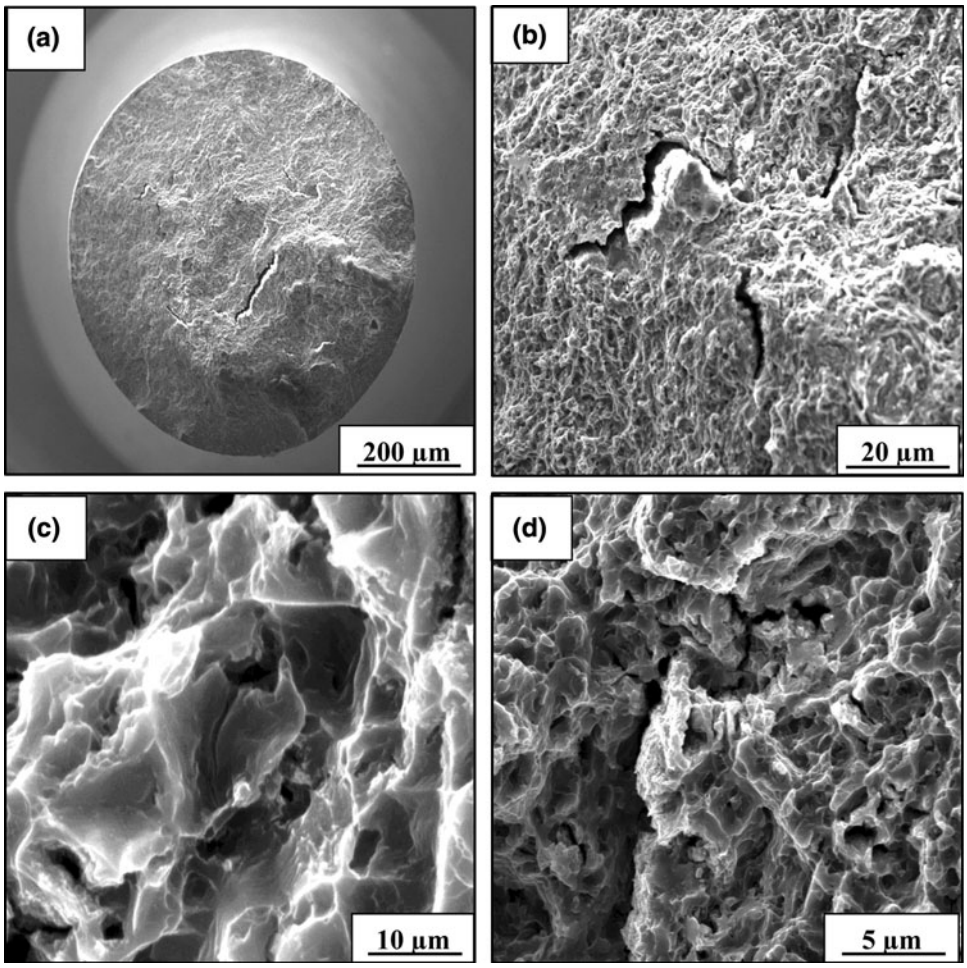

Fig. 2 Scanning electron micrographs of magnesium alloy AZ31 deformed in tension to failure showing: (a) Overall morphology of failure. (b) Macroscopic cracks of varying size and orientation on the tensile fracture surface. (c) Fine microscopic cracks intermingled with microscopic voids and dimples features reminiscent of locally brittle and ductile failure mechanisms. (d) Microscopic cracks voids of varying size and shape and dimples covering the overload surface

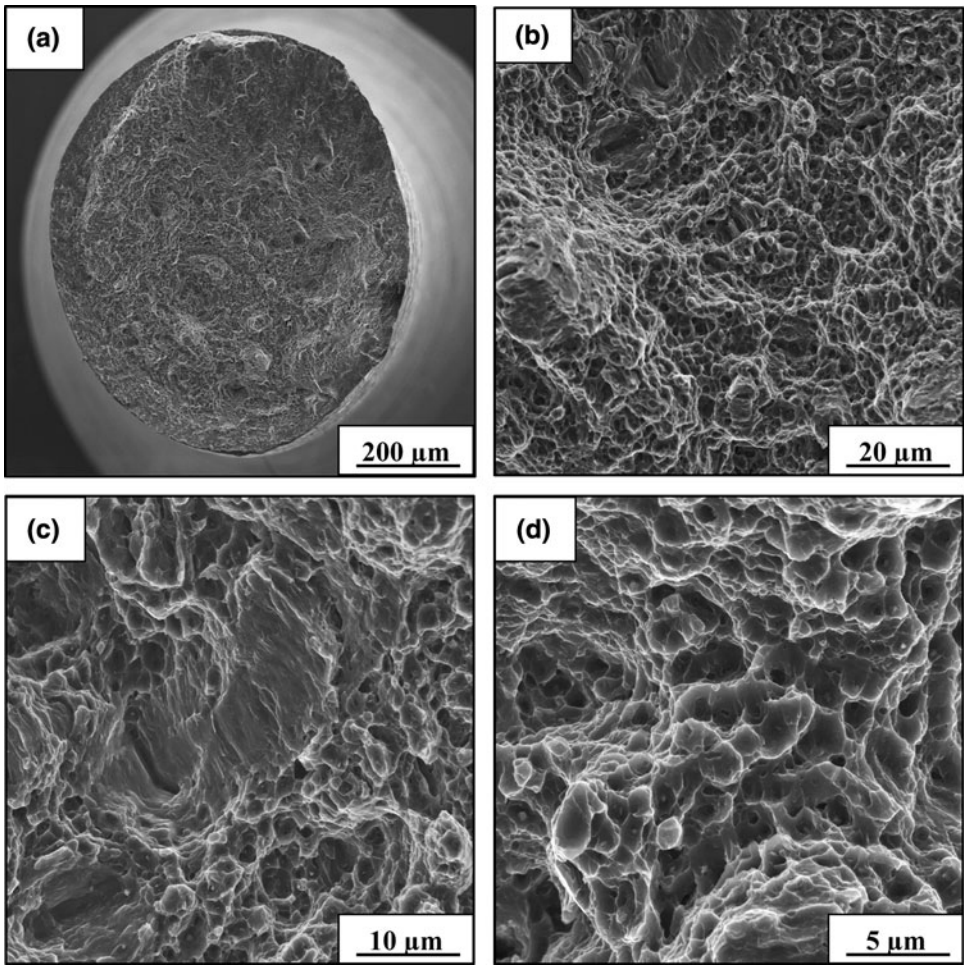

Fig. 3 Scanning electron micrographs of AZ31 reinforced with particulates of Al_2O_3, deformed in tension, showing: (a) Overall morphology of failure. (b) High magnification observation of (a) showing intrinsic features on the tensile fracture surface. (c) Pockets of flat and near-featureless transgranular region surrounded by microscopic voids and a healthy population of ductile dimples. (d) Voids and dimples on the overload fracture surface reminiscent of locally ductile failure mechanisms

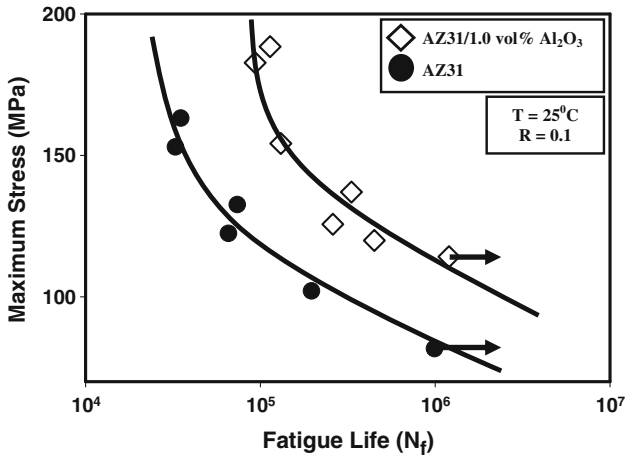

Fig. 4 Variation of maximum stress (σ_{max}) with fatigue life (N_f) for AZ31 and AZ31/1.5 vol.% Al_2O_3 at load ratio ($R = \sigma_{min}/\sigma_{max}$) of 0.1

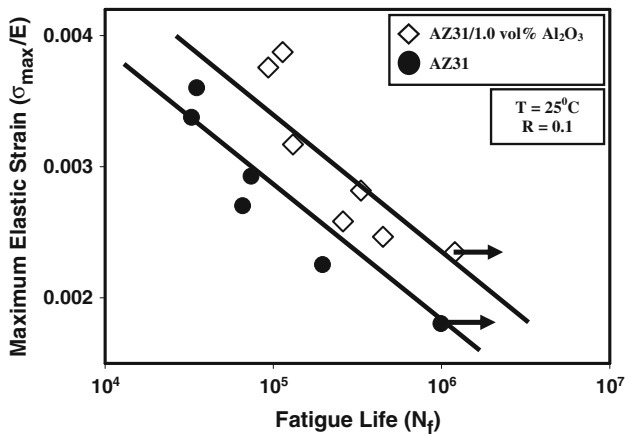

Fig. 5 Variation of maximum elastic strain (σ_{max}/E) with fatigue life (N_f) for AZ31 and AZ31/1.5 vol.% Al_2O_3 at load ratio ($R = \sigma_{min}/\sigma_{max}$) of 0.1

tensile and fatigue samples. Observations were made over a range of magnifications to identify the macroscopic fracture mode and to concurrently establish the microscopic mechanisms governing failure. Samples for observation were obtained from the fully deformed and failed test specimens by sectioning parallel to the fracture surface.

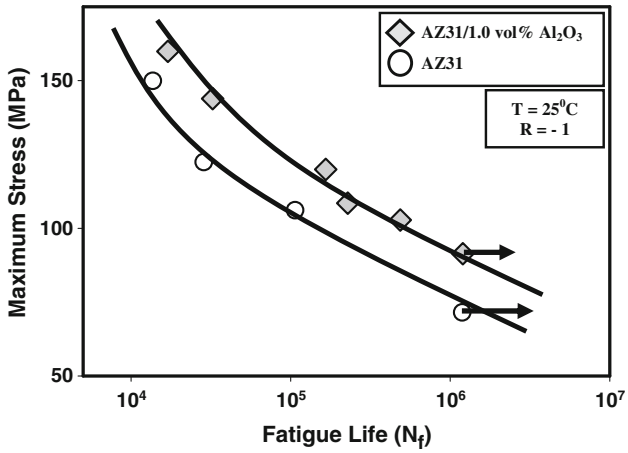

Fig. 6 Variation of maximum stress (σ_{max}) with fatigue life (N_f) for AZ31 and AZ31/1.5 vol.% Al_2O_3 at load ratio ($R = \sigma_{min}/\sigma_{max}$) of −1

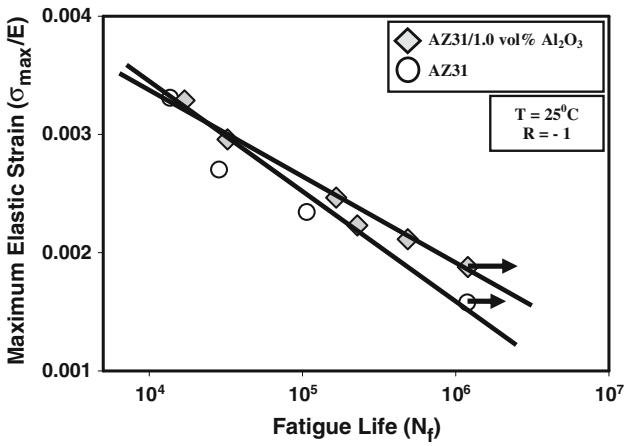

Fig. 7 Variation of maximum elastic strain (σ_{max}/E) with fatigue life (N_f) for AZ31 and AZ31/1.5 vol.% Al_2O_3 at load ratio ($R = \sigma_{min}/\sigma_{max}$) of −1

4. Results and Discussion

4.1 Microstructure

The optical microstructures of the monolithic alloy AZ31 and nano-alumina particle-reinforced composite was taken using bright field illumination techniques and shown in Fig. 1. Both the unreinforced alloy and the reinforced magnesium alloy revealed a poly-grained structure but with a noticeable difference in their grain size. The nano-alumina particle-reinforced magnesium alloy revealed a small yet observable decrease in grain size (Fig. 1b) when compared to the monolithic counterpart (AZ31) (Fig. 1a). The observed refinement in grain size of the nano-alumina particulate-reinforced magnesium alloy-based composite is ascribed to the interactive influences of the following:

(a) High extrusion temperature of 623 K ($T \sim 0.7\ T_m$) resulting in dynamic recrystallization (DRX) (Ref 26, 27), and
(b) Presence of a near-uniform dispersion of the reinforcing Al_2O_3 nanoparticles, which act as potential heterogeneous nucleation sites during solidification, made possible by minimum gravity related segregation due to an appropriate selection of the stirring parameters during processing of the composite (Ref 21).

A duplex microstructure consisting of light-colored alpha (α) phase and the dark-colored eutectic phase (β) (distributed at and along the grain boundaries) were identified in both the unreinforced magnesium alloy and the reinforced magnesium alloy composite. Earlier studies have identified the eutectic phase (β) in candidate magnesium-base alloys, using the X-ray diffraction technique, to be the intermetallic particle $Mg_{17}Al_{12}$ (Ref 28-30). A higher volume fraction of the eutectic phase (β) was observed in the reinforced magnesium alloy (Fig. 1b) when compared one-on-one with the unreinforced magnesium alloy counterpart (Fig. 1a). No attempt was made in this study to quantify the exact volume fraction of the two phases (α and β) in the unreinforced alloy and the reinforced nanocomposite.

4.2 Microhardness

The microhardness values tabulated in Table 1 reveal a noticeable increase, i.e., 41 pct, in hardness of the composite when compared to the monolithic counterpart. An increase in hardness arising from an integration of the nanoparticle reinforcement with the magnesium alloy metal matrix has been reported in alumina fiber reinforced Mg-4.2% Zn-RE alloy, alumina (Al_2O_3)-reinforced elemental magnesium (Ref 31, 32), nano-alumina-reinforced AZ31 (Ref 10, 11, 27), silicon carbide (SiC) (Ref 33) or copper particle-reinforced magnesium alloy AZ91, and SiC particulate-reinforced magnesium alloy AZ92 (Ref 34).

The observed increase in hardness can be ascribed to the conjoint and mutually interactive influences of (i) strengthening mechanisms arising from restricting or impeding the motion of dislocation, (ii) presence and near-uniform distribution of hard second-phase (Al_2O_3) particles in the magnesium alloy metal matrix achieved by optimum processing, and (iii) a refinement in grain size observed in the magnesium alloy metal matrix due to "pinning" effect of the nanoreinforcement (Ref 4, 10, 11, 31).

4.3 Tensile Deformation and Fracture Behavior

The uniaxial tensile test results and resultant fracture behavior of the extruded monolithic alloy (AZ31) and nano-alumina particle-reinforced composite are summarized in Table 2. The values reported are the mean based on duplicate tests. An attempt is made to understand the synergistic and/or mutually interactive influences of the macroscopic and fine microscopic mechanisms governing deformation under tensile load.

The following observations are drawn from the test results.

1. A 7% increase in the Young's Modulus (E) of the AZ31/1.5 vol.% Al_2O_3 composite when compared to the monolithic alloy (AZ31).
2. A 12% increase in yield strength of the composite when compared to the monolithic counterpart.
3. The nanoparticle-reinforced composite showed a reduction in percent elongation by 22% when compared to the monolithic counterpart (AZ31). However, tensile ductility as measured by reduction in test specimen cross-sectional area decreased by only 11%.

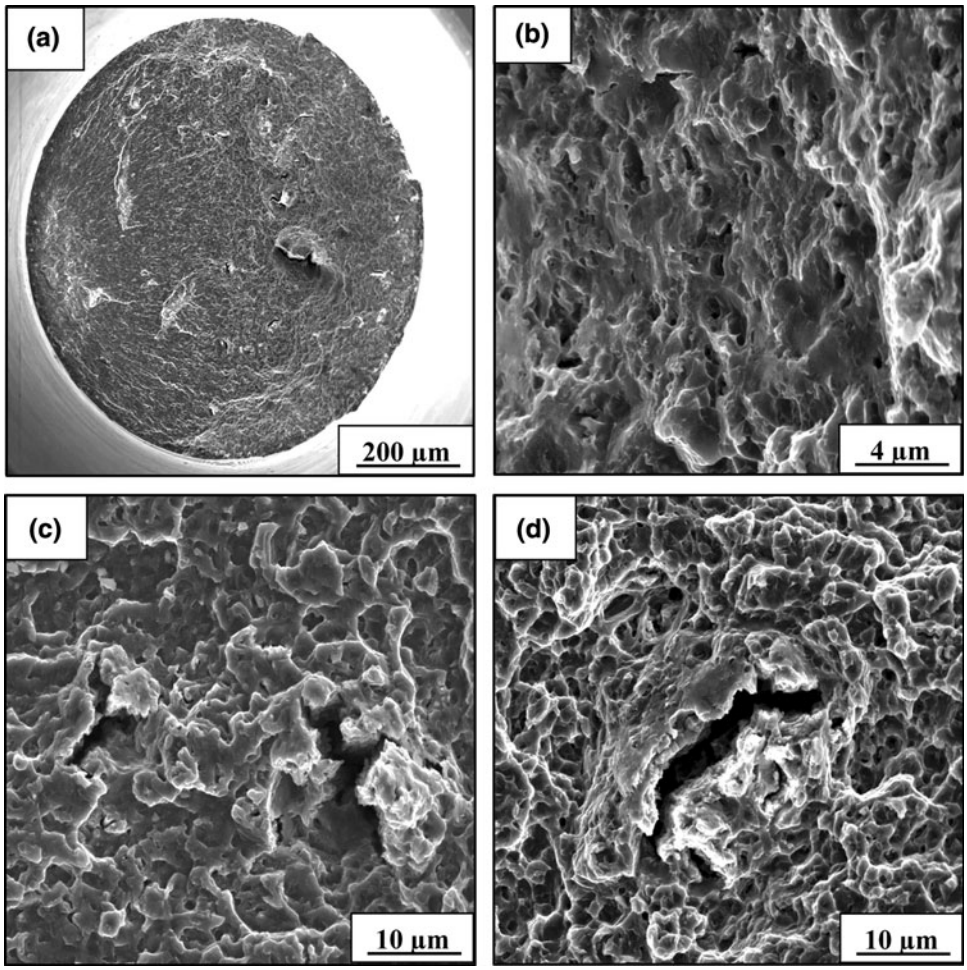

Fig. 8 Scanning electron micrographs of the high cycle fatigue fracture surface of AZ31 deformed at maximum cyclic stress of 152.72 MPa at load ratio of 0.1, fatigue life of 32,940 cycles, showing the following: (a) Overall morphology of failure. (b) High magnification observation of the region of crack initiation and early microscopic growth showing a random distribution of fine microscopic voids. (c) The region of stable crack growth showing fine microscopic cracks and an absence of striations. (d) Microcracking surrounded by dimples of varying size in the region of overload

A higher increase in microhardness between the two candidate materials when compared to the observed increase in strength obtained from the global tensile test can be ascribed to the role played by defects sick as microscopic cracks, microvoids and macroscopic voids in governing macroscopic mechanical behavior compared to the highly localized nature of the microindent and resultant hardness (i.e., microhardness).

The observed improvement in mechanical properties, i.e., elastic modulus and yield strength, is be ascribed to interactions at the fine microscopic level between (a) matrix and nanoparticle reinforcements (Ref 1, 4, 33), and (b) the β phase ($Mg_{17}Al_{12}$) and the matrix (Ref 35, 36). These interactions result in a mismatch in strain generating a higher density of dislocations and localized stress in the matrix immediately around the reinforcement, thus contributing to strengthening of the material. The observed reduction in ductility (documented in terms of percent elongation and percent reduction in test specimen cross-sectional area) of the alumina particle-reinforced composite when compared to the unreinforced counterpart (AZ31) is partially attributed to a high volume of the eutectic β ($Mg_{17}Al_{12}$) phase observed both at and along the grain boundaries of the composite (Fig. 1b). During far-field tensile deformation, there is a tendency for the fine microscopic cracks to nucleate at the interface between the α phase (body-centered cubic structure) and the matrix (predominantly a hexagonal closed packed crystal structure) due to strain incompatibility. With continued loading the fine microscopic cracks grow and eventually coalesce to form one or more macroscopic cracks. Concurrent growth of both the fine microscopic and macroscopic cracks eventually culminates in failure (Ref 7, 37, 38).

The tensile fracture behavior of the monolithic alloy AZ31 is shown in Fig. 2. The overall morphology of the failed sample is shown in Fig. 2(a). Higher magnification observation of the crack initiation region reveals macroscopic cracks of varying size and orientation (Fig. 2b). At progressively higher allowable magnifications of the SEM revealed a combination of population of dimples, fine microscopic voids and isolated microscopic cracks. These features are indicative of the occurrence of both ductile and brittle failure mechanisms at the microscopic level (Fig. 2c). Microscopic cracks and voids of varying sizes with a noticeable population of dimples were observed in the region of overload indicative of "locally" ductile and brittle failure mechanisms (Fig. 2d).

Observations of the tensile fracture surface of the magnesium alloy AZ31 reinforced with nanoparticulates of Al_2O_3 are shown in Fig. 3. Overall morphology taken of the fracture

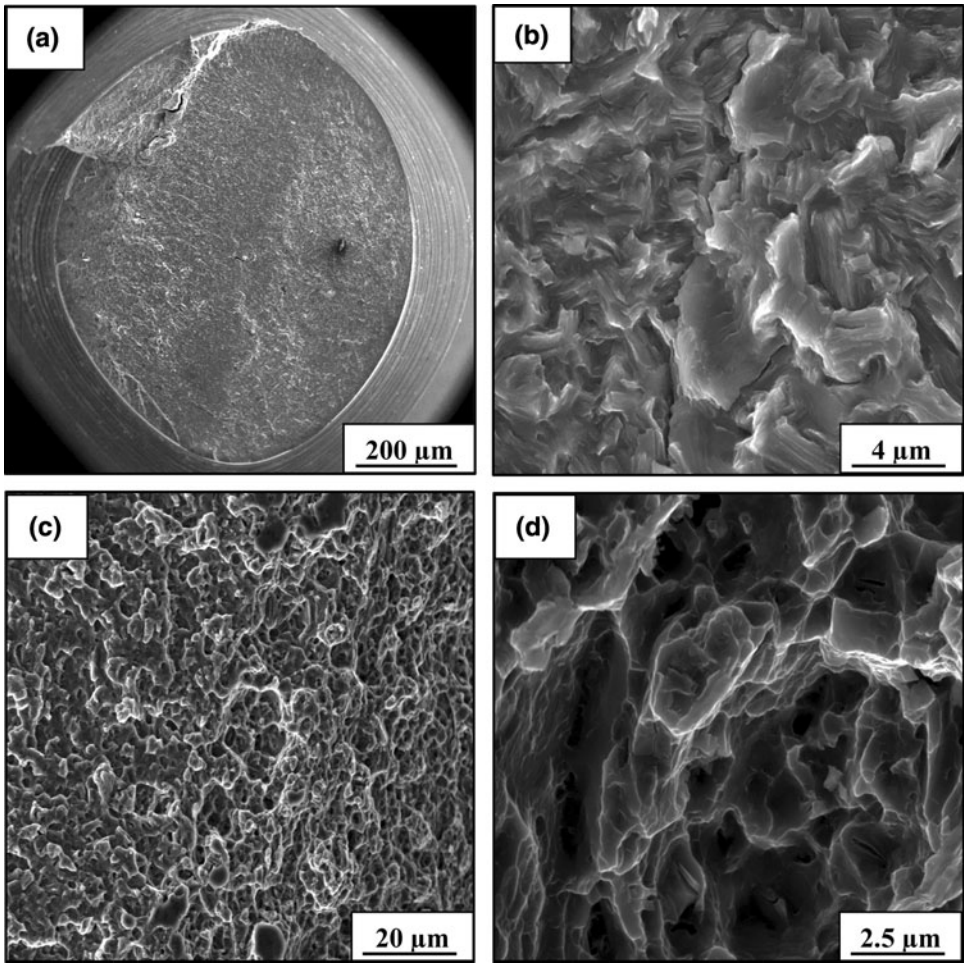

Fig. 9 Scanning electron micrographs of the high cycle fatigue fracture surface of AZ31 deformed at maximum cyclic stress of 102 MPa at load ratio of 0.1, fatigue life of 197,813 cycles, showing the following: (a) Overall morphology of failure. (b) A random dispersion of fine striations in the region of early microscopic crack growth. (c) The region of unstable crack growth immediately prior to overload covered with population of fine microscopic voids and dimples. (d) Morphology, size, and distribution of dimples on the overload fracture surface

surface is shown in Fig. 3(a). The tensile fracture surface region revealed an observable population of dimples (Fig. 3b). At the higher allowable magnifications the transgranular region was observed to be flat, near-featureless and surrounded by an observable population of fine microscopic voids and pockets of dimples (Fig. 3c). Voids of varying size and shape intermingled with dimples were found covering the region of tensile overload (Fig. 3d).

4.4 Cyclic Stress-Controlled High Cycle Fatigue Behavior

The results of cyclic stress-controlled high cycle fatigue are shown in Fig. 4, 5, 6, and 7. The strains that the materials underwent during the test were predominantly elastic and the maximum applied stresses were well below the tensile yield stress of the candidate material. Most of the fatigue life under conditions of stress-controlled fatigue is spent in crack initiation. The test provides a useful measure of the endurance limit of the material at the chosen load ratio.

4.4.1 Load Ratio $R = 0.1$ [$R = \sigma_{minimum}/\sigma_{maximum}$]. The results of the stress-controlled high cycle fatigue behavior of monolithic AZ31 and AZ31/1.5 vol.% Al_2O_3 under tension-tension type loading [$R = 0.1$] and in stress range of 80 MPa to 190 MPa are shown in Fig. 4 and 5. The variation between maximum stress ($\sigma_{maximum}$) versus cycles to failure (N_f) is shown in Fig. 4. The samples that did not fail are marked by arrows. The endurance limit of the nanocomposite was 110 MPa while the monolithic alloy showed an endurance limit of 81 MPa, both taken at 10^6 cycles. The nanoparticle-reinforced composite revealed an improvement of 36% in endurance limit over the monolithic counterpart. To better understand the specific role of the high stiffness reinforcement on cyclic fatigue response, the maximum stress versus fatigue life curve was replotted in terms of elastic strain amplitude ($\sigma_{maximum}/E$) and is as shown in Fig. 5. The composite microstructure showed better resistance to fatigue-induced deformation when compared to the monolithic (AZ31) counterpart though degradation in cyclic fatigue life was evident in both the materials with an increase in maximum elastic strain.

4.4.2 Load Ratio $R = -1$. To understand the behavior of the two materials under fully reversed loading conditions ($R = -1$; tension-compression) high cycle fatigue tests were performed over the maximum stress ranging from 71 and 160 MPa. The endurance limit for the AZ31 magnesium alloy, taken at 1.2×10^6 cycles, was 71 MPa, while that of the nano-alumina particle-reinforced composite was 91 MPa taken at 1.2×10^6 cycles (Fig. 6). Under conditions of fully reversed loading, the nano-alumina particle-reinforced composite fared

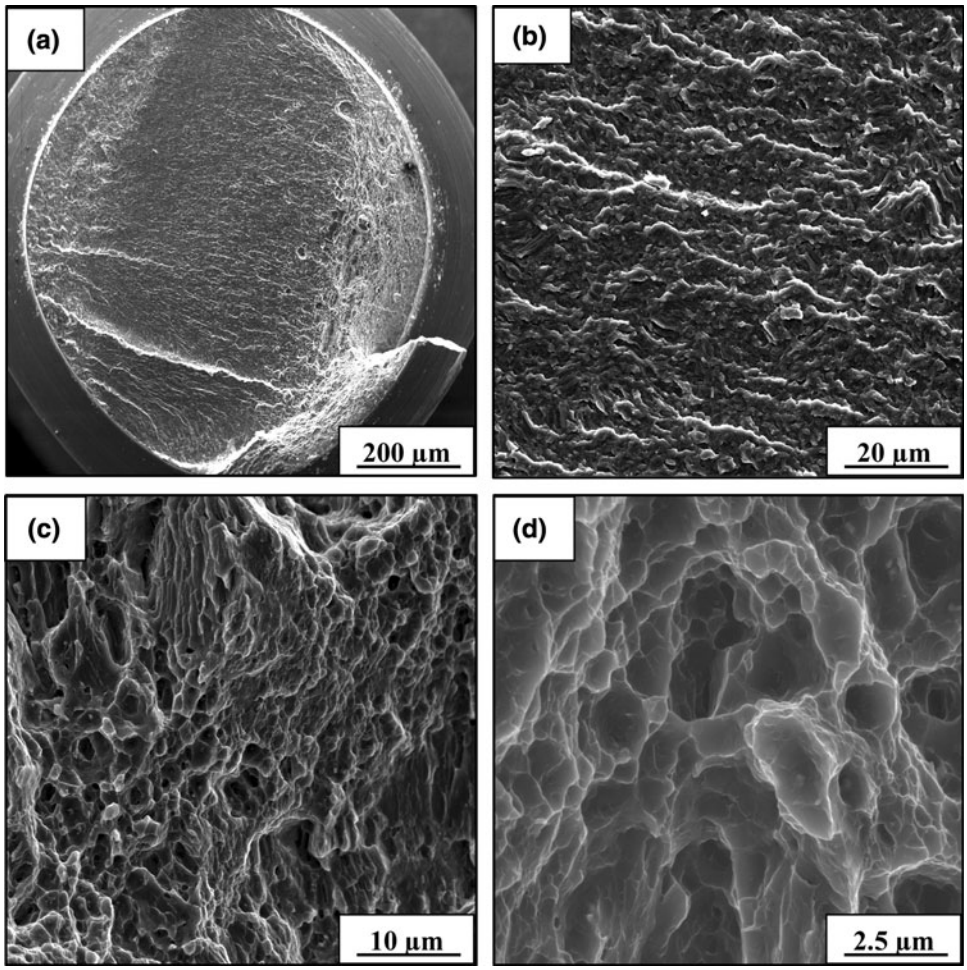

Fig. 10 Scanning electron micrographs of the high cycle fatigue fracture surface of AZ31 reinforced with Al_2O_3 particulates and deformed at maximum cyclic stress of 182.72 MPa at load ratio of 0.1, fatigue life of 93,280 cycles, showing the following: (a) Overall morphology of failure. (b) High magnification observation of the region of stable crack growth, almost flat and lacking in discernible features. (c) A healthy population if microscopic voids and dimples in the region of unstable crack growth. (d) Voids of varying size intermingled with a healthy population of dimples in the region of unstable crack growth and overload

better showing an improvement of 28% in endurance limit. Variation of maximum elastic strain ($\sigma_{maximum}/E$) with cyclic fatigue life (N_f) is shown in Fig. 7. At the lower values of maximum strain and resultant enhanced fatigue life, the unreinforced monolithic alloy (AZ31) revealed a noticeable degradation in cyclic fatigue life (N_f) when compared to the nanocomposite.

The reasons responsible for the observed improvement in fatigue behavior of the nano-alumina particle-reinforced composite over the unreinforced alloy (AZ31) can be ascribed to an interaction between the particulate reinforcements and the metal matrix, intrinsic microstructural effects and microscopic mechanisms delaying crack initiation and resultant crack growth.

1. AZ31/1.5 Al_2O_3 composite showed a refined microstructure when compared to the monolithic counterpart (as seen in Fig. 1). This contributed in a noticeable way in retarding crack initiation with a concomitant improvement in cyclic fatigue life.
2. Under the influence of far-field tensile stresses the high-modulus, high-strength alumina reinforcement carried most of the load at the fine microscopic level and thus the constituents of the composite experienced a lower strain when compared to the monolithic alloy (AZ31).
3. Improved compatibility (wetting) between the reinforcing nanoparticle reinforcements and the magnesium alloy matrix was made possible by the optimum processing conditions helped in forming a compatible interface between the composite constituents thereby facilitating load transfer from the soft and ductile magnesium alloy metal matrix to the hard, brittle and elastically deforming alumina particle reinforcements without the occurrence of debonding.
4. A proper selection of the stirring parameters during processing of the composite ensured that there was an absence of agglomeration of the reinforcing particulates, which would have otherwise acted as sites for the nucleation of cracks.

4.5 Cyclic Fatigue Fracture Behavior

4.5.1 Load Ratio [*R*] = 0.1. *Monolithic Magnesium Alloy AZ31.* Key features of the test specimen that was cyclically deformed at a maximum stress of 153 MPa and a resultant fatigue life of 32,940 cycles are shown in Fig. 8.

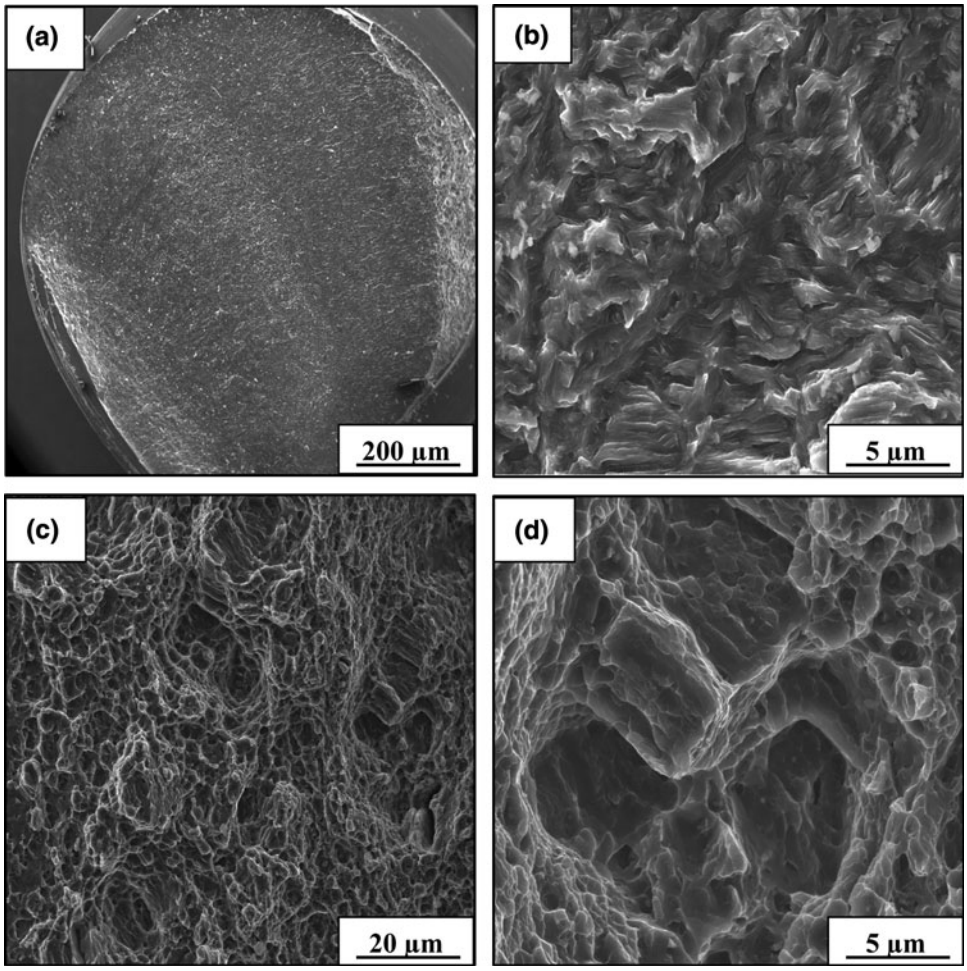

Fig. 11 Scanning electron micrographs of the high cycle fatigue fracture surface of AZ31 reinforced with Al_2O_3 particulates and deformed at maximum cyclic stress of 119.91 MPa at load ratio of 0.1, fatigue life of 448,630, showing the following: (a) Overall morphology of failure. (b) High magnification observation of the region of stable crack growth showing pockets of fine and shallow striations reminiscent of localized microplastic deformation. (c) High magnification observation of the fracture surface in the region of stable crack growth adjacent to unstable crack growth. (d) Shallow striations present in pockets surrounded by a population of voids and dimples in the region of unstable crack growth

Overall morphology of the failed surface is as shown in Fig. 8(a), and is essentially normal to the far-field stress axis comprising distinct regions of early microscopic crack growth and tensile overload. The region of early macroscopic crack growth when examined at higher allowable magnifications of the SEM revealed a random distribution of fine microscopic voids (Fig. 8b). The region of stable crack growth revealed numerous fine microscopic cracks and an absence of striations, as shown in Fig. 8(c), indicative of locally brittle failure mechanism. The region of overload revealed features that were reminiscent of the occurrence of "locally" ductile and brittle failure mechanisms as evident by the fine microscopic cracks surrounded by an observable population of dimples of varying size (Fig. 8d).

At a lower maximum stress of 102 MPa and resultant fatigue life of 197,813 cycles the key features of the deformed sample are shown in Fig. 9. Overall morphology of the fracture surface was at an inclination to the far-field stress axis (Fig. 9a). The region of early crack growth (Fig. 9b) revealed a random dispersion of fine striations indicative of 'localized' microplastic deformation. The region of unstable crack growth prior to overload was observed to be covered with population of fine microscopic voids and dimples indicative of a predominantly "locally" ductile failure mechanism (Fig. 9c). The region of overload when observed at the higher allowable magnifications of the SEM revealed a healthy population of dimples (Fig. 9d).

Alumina Particulate (1.5 vol.%) Reinforced AZ31 Alloy. Key features of the nano-alumina particle-reinforced composite sample when cyclically deformed at 183 MPa resulting in a fatigue life of 93,280 cycles are shown in Fig. 10. Overall morphology of the fracture surface was at an inclination to the far-field stress axis showing distinct regions of crack initiation, growth and overload (Fig. 10a). High magnification observation of region of stable crack growth was essentially flat lacking any discernible features (Fig. 10b). The region of unstable crack growth revealed a noticeable population of microscopic voids coupled with an absence of fine microscopic cracks indicative of "Locally" ductile failure (Fig. 10c). High magnification observation of the overload region (Fig. 10d) revealed an observable population of dimples and voids indicative of highly "localized" plastic deformation that is aided by the steep stress gradients immediately around the reinforcing alumina particulates.

At a lower maximum stress of 120 MPa and resultant fatigue life of 448,630 cycles the key features observed on the

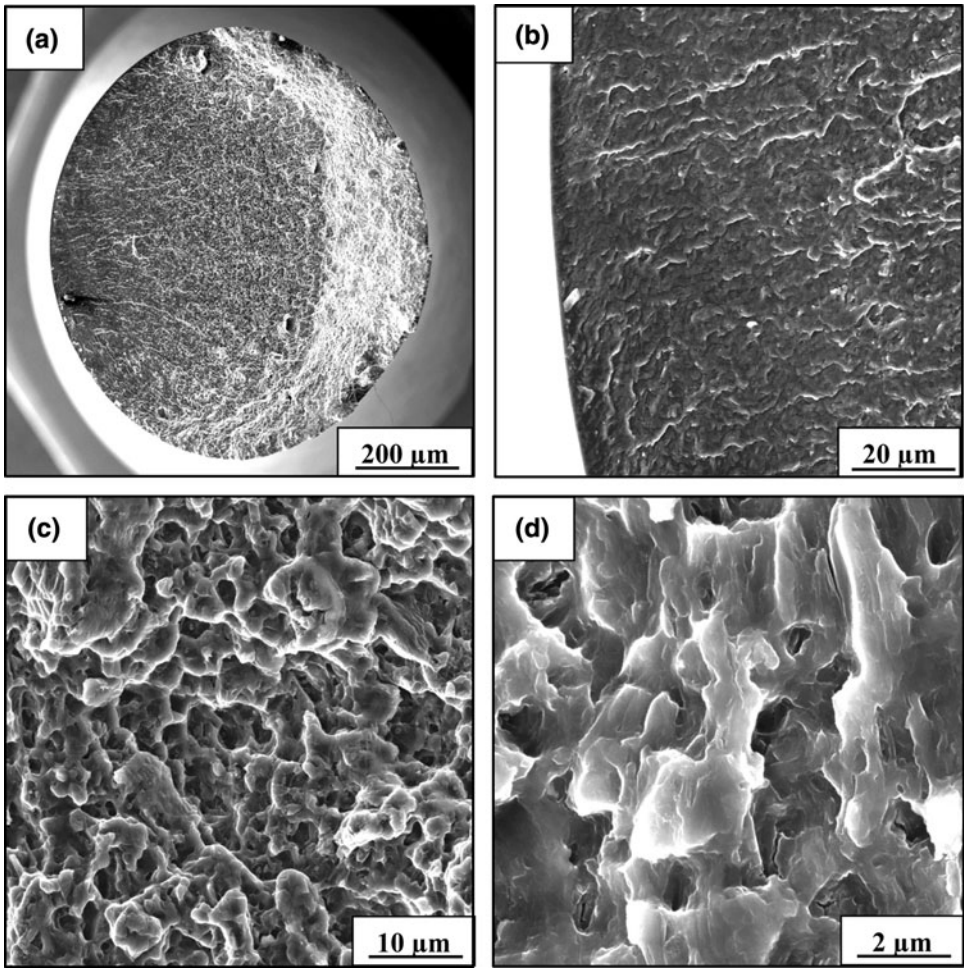

Fig. 12 Scanning electron micrographs of the high cycle fatigue fracture surface of AZ31 cyclically deformed at maximum stress of 149.67 MPa and load ratio of -1.0 and fatigue life of 13,802 cycles, showing: (a) Overall morphology. (b) High magnification of (a) showing the fracture surface in the region of early crack growth. (c) The region of unstable crack growth showing a healthy population of voids of varying size. (d) The overload fracture region showing an array of fine microscopic cracks and shallow dimples reminiscent of locally brittle and ductile failure mechanisms

deformed composite sample are shown in Fig. 11. Overall morphology of failure was essentially flat and normal to major stress (Fig. 11a). At gradually higher magnifications microplastic deformation was evident in the region of stable crack growth as indicated by the presence of pockets of fine and shallow striations (Fig. 11b). Gradual high magnification observation of the fracture surface in the region of stable crack growth adjacent to unstable crack growth revealed a sizeable population of dimples and voids of varying size and shape (Fig. 11c). The region adjacent to unstable crack growth revealed well distributed population of shallow voids and very fine yet isolated microscopic cracks suggesting the occurrence of both ductile and brittle failure mechanisms (Fig. 11d).

4.5.2 Load Ratio [*R*] = −1. *Unreinforced Magnesium Alloy AZ31.* Key features of the monolithic sample that was cyclically deformed at a maximum stress of 150 MPa and under fully reversed loading with a resultant fatigue life of 13,802 cycles are shown in Fig. 12. Macroscopic observations of the fracture surface revealed it to be rough and at an inclination with respect to the far-field stress axis (Fig. 12a) showing distinct regions of crack initiation, stable crack growth, and tensile overload. The transgranular regions when observed at high magnifications revealed to be essentially flat and near-featureless (Fig. 12b). The region of unstable crack growth (Fig. 12c) immediately prior to tensile overload was covered with a noticeable population of voids of varying size reminiscent of locally operating ductile failure mechanisms. The region of overload was covered with an array of fine microscopic cracks and shallow dimples reminiscent of ''locally'' brittle and ductile failure mechanisms (Fig. 12d).

For the test specimen that was cyclically deformed at a lower maximum stress of 102 MPa and a resultant fatigue life of 240,921 cycles the key features of the deformed monolithic sample are shown in Fig. 13. Overall morphology of failure revealed to be normal to the far-field stress axis and comprising of a smooth region indicative of fatigue and a rough region indicative of overload (Fig. 13a). Higher magnification observation of the region of early microscopic crack growth revealed the surface to be rough with ''pockets'' of transgranular regions sandwiched between the fine microscopic cracks (Fig. 13b). The region of stable crack growth revealed a random dispersion of shallow striations indicative of the occurrence of microplastic deformation at the 'local' level (Fig. 13c). The region of stable crack growth revealed evidence of macroscopic cracks

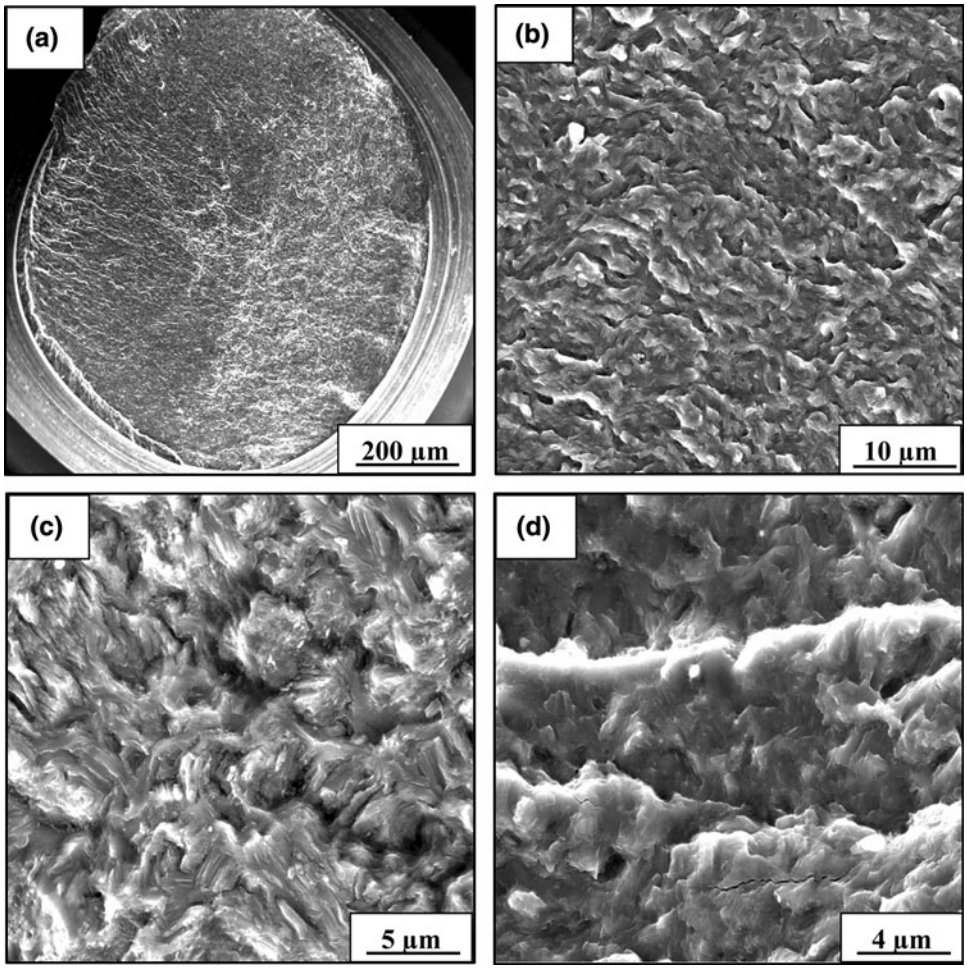

Fig. 13 Scanning electron micrographs of the high cycle fatigue fracture surface of magnesium alloy AZ31 cyclically deformed at maximum stress of 101.82 MPa, at load ratio of −1 and resultant fatigue life of 240,921 cycles, showing: (a) Overall morphology of failure. (b) High magnification observation if (a) showing intrinsic features in the region of early microscopic crack growth. (c) Shallow striations randomly dispersed in the region of stable crack growth. (d) The region of unstable crack growth showing macroscopic and fine microscopic cracks

and an array of fine microscopic cracks (Fig. 13d). These features are clearly indicative of the occurrence of both brittle and ductile failure mechanisms at the fine microscopic level.

Reinforced magnesium alloy AZ31/1.5 vol.% Al_2O_3. Observation made on the fracture surface of the cyclically deformed nano-alumina particle-reinforced composite sample deformed at a maximum stress of 160 MPa and resultant fatigue life of 16,980 cycles is shown in Fig. 14. Overall morphology of the fracture surface was at an inclination to the far-field stress axis revealing distinct regions of crack initiation, propagation and tensile overload (Fig. 14a). An observation of the region of stable crack growth at gradually higher magnifications of the SEM revealed fine microscopic cracks representative of "locally" brittle failure mechanisms (Fig. 14b). In the domain of unstable crack growth was observed a population of microscopic voids intermingled with an array of microscopic cracks suggesting the occurrence of both ductile and brittle deformation in this region (Fig. 14c). Just prior to the region of tensile overload was observed a population of shallow dimples intermingled with an array of microscopic voids (Fig. 14d). These intrinsic features are indicative of the occurrence of 'locally' ductile failure mechanisms.

The key features observed for the composite material that was cyclically deformed at a maximum stress of 108 MPa with a resultant fatigue life of 227,796 cycles is shown in Fig. 15. Overall morphology was at an inclination to the far-field stress axis (Fig. 15a). High magnification observation of the region of stable crack growth revealed an array of extremely fine microscopic cracks (Fig. 15b). The region prior to the onset of unstable crack growth revealed numerous cracks of varying sizes suggesting the occurrence of 'locally' brittle failure (Fig. 15c). In the region of stable crack growth (Fig. 15d), an array of microscopic voids intermingled with shallow dimples and random pockets of shallow striations was observed.

5. Conclusions

Based on a study aimed at understanding the influence of nanosize alumina particulate reinforcements on hardness, tensile properties, cyclic fatigue and final fracture behavior of magnesium alloy (AZ31), the following are the key findings:

1. Overall grain size of the reinforced composite was finer when compared to monolithic AZ31 counterpart and is

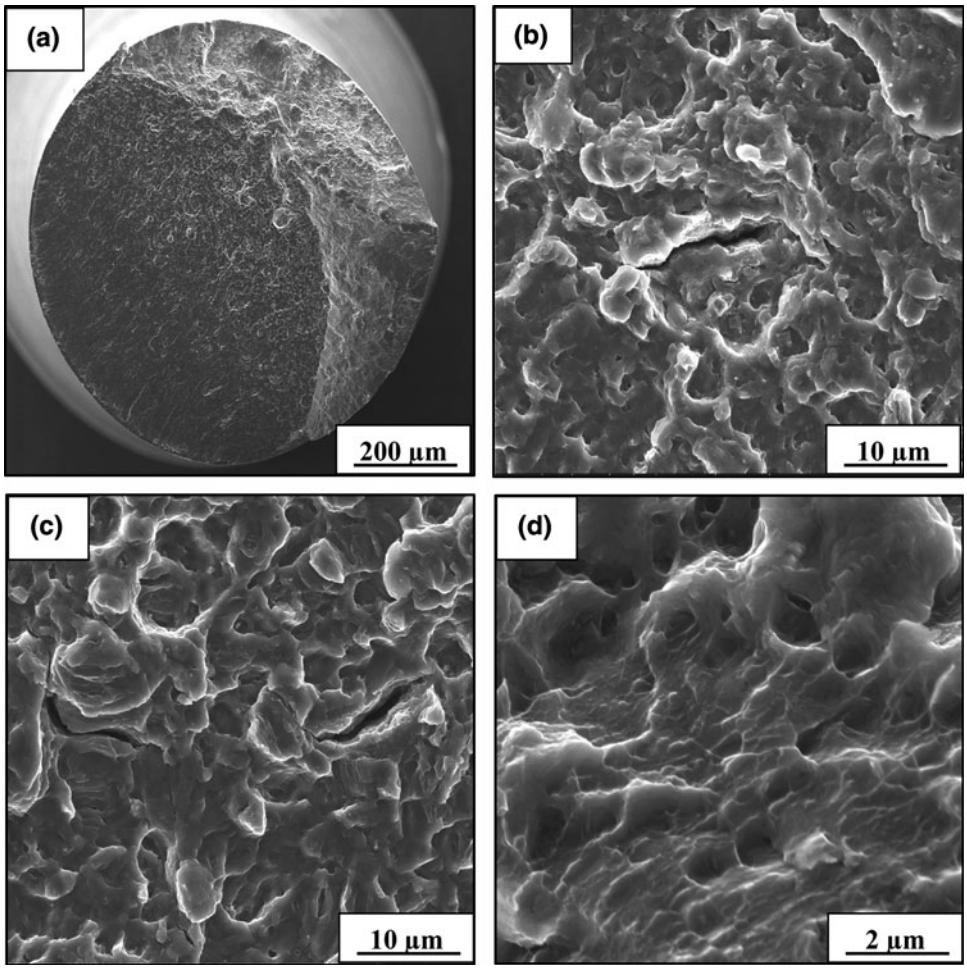

Fig. 14 Scanning electron micrographs of the high cycle fatigue fracture surface of AZ31 reinforced with Al_2O_3 particulates and deformed at maximum cyclic stress of 159.88 MPa at load ratio of −1.0, fatigue life of 16,980 cycles, showing the following: (a) Overall morphology of failure. (b) Microscopic crack in the predominantly transgranular region in the domain of stable crack growth. (c) A population of microscopic voids of varying size and fine microscopic cracks in the region of unstable crack growth. (d) The shallow nature of dimples and population of microscopic voids in the region of unstable crack growth prior to overload

ascribed to the synergistic influence of dynamic recrystallization (DRX) during high temperature extrusion and the role of pinning effect of the uniformly distributed alumina particulates made possible by optimum processing.

2. Compared to the monolithic alloy (AZ31) the nano-alumina particulate-reinforced composite revealed an observable improvement in microhardness of 36% and a small improvement in both elastic modulus (7%) and yield strength (12%). These enhancements can be attributed to the conjoint and mutually interactive influences of: (i) a refined microstructure (grain size), (ii) high modulus of the reinforcing phase (Al_2O_{3p}), and (iii) particulate reinforcement-metal matrix compatibility resulting in proper load transfer between the composite constituents, i.e., metal matrix and particulate reinforcements.
3. The composite revealed a loss in ductility when compared to the monolithic counterpart (AZ31). This is ascribed to the presence of a higher volume of the eutectic $Mg_{17}Al_{12}$ (β) phase that was present mainly along the grain boundaries of the composite.
4. The composite revealed a higher endurance limit (taken at 10^6 cycles). A 36 pct improvement at load ratio of 0.1 and 28 pct improvement at a load ratio of −1, when compared one-on-one with the monolithic alloy AZ31. This suggests a favorable influence of the nanoparticle-reinforced magnesium alloy metal matrix in delaying crack initiation and concurrently retarding crack propagation or growth through the microstructure.
5. Intrinsic features on the fatigue surface of both the unreinforced and reinforced alloys were found to vary with load ratio, maximum stress and cyclic fatigue life. The region of overload of the composite material revealed a higher population of dimples and fine microscopic voids indicative of "locally" ductile deformation. The shallow and distinct striations observed in the monolithic alloy are indicative of the occurrence of microplastic deformation at the local level.

Acknowledgments

The authors express and extend most sincere thanks and appreciation to the two 'unknown' reviewers for their comments, corrections and suggestions. These have been included/incorporated

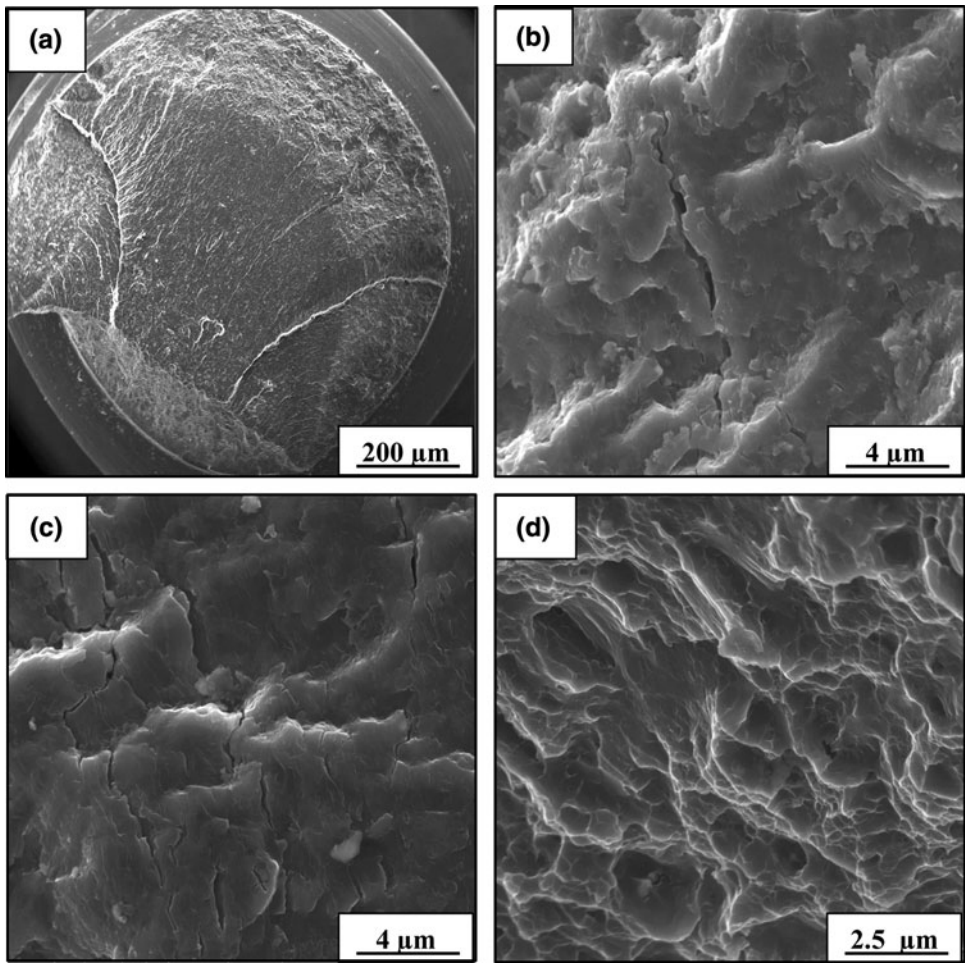

Fig. 15 Scanning electron micrographs of the high cycle fatigue fracture surface of AZ31 reinforced with Al_2O_3 particulates and deformed at maximum cyclic stress of 108.49 MPa at load ratio of −1.0, fatigue life of 227,796 cycles, showing the following: (a) Overall morphology of failure. (b) An array of fine microscopic cracks in the region of stable crack growth. (c) An array of fine microscopic cracks of varying size in the region of stable crack growth immediately prior to the onset of unstable crack growth. (d) The shallow nature of striations present in small pockets, microscopic voids of varying size and shallow dimples in the region of unstable crack growth

and addressed in the revised manuscript and have helped add to improving the overall quality and content.

References

1. D.J. Lloyd, Particle reinforced aluminum and magnesium matrix composites, *Int. Mater. Rev.*, 1994, **39**, p 1–24
2. T.S. Srivatsan, T.S. Sudarshan, and E.J. Lavernia, Processing of discontinuously-reinforced metal matrix composites by rapid solidification, *Prog. Mater Sci.*, 1995, **39**, p 317–409
3. F. Czerwinski, Z. Trojanova, Z. Szaraz, P. Palcek and M. Chalupova, Ed., *Magnesium Alloys—Design, Processing and Properties*, InTech, 2011
4. H.Z. Ye and X.Y. Liu, Review of Recent Studies in Magnesium Matrix Composites, *J. Mater. Sci.*, 2004, **39**, p 6153–6171
5. Z. Trojanova, V. Gartnerova, P. Lukac, and Z. Drozd, Mechanical Properties of Mg Alloys Composites Reinforced with Short Saffil® Fibers, *J. Alloys Compd.*, 2004, **378**(1–2), p 19–26
6. Y. Morisada, H. Fuji, T. Nagaoka, and M. Fukusumi, Effect of Friction Stir Processing with SiC Particles on Microstructure and Hardness of AZ31, *Mater. Sci. Eng., A*, 2006, **433**, p 50–54
7. J.-J. Wang, J.-H. Guo, and L.-Q. Chen, TiC/AZ91D composites fabricated by in situ reactive infiltration process and its tensile deformation, *Trans. Nonferr. Met. Soc. China*, 2006, **16**(4), p 892–896
8. K.F. Ho, M. Gupta, and T.S. Srivatsan, The Mechanical Behavior of Magnesium Alloy AZ91 Reinforced with Fine Copper Particulates, *Mater. Sci. Eng., A*, 2004, **369**(1–2), p 302–308
9. M. Habibnejad-Korayema, R. Mahmudi, and W.J. Pooleb, Enhanced Properties of Mg-Based Nano-composites Reinforced with Al2O3 Nano-particles, *Mater. Sci. Eng., A*, 2009, **519**, p 198–203
10. Q.B. Nguyen and M. Gupta, Increasing Significantly the Failure Strain and Work of Fracture of Solidification Processed AZ31B Using Nano-Al_2O_3 Particulates, *J. Alloys Compd.*, 2008, **459**, p 244–250
11. M. Paramsothy, S.F. Hasan, N. Srikanth, and M. Gupta, Enhancing Tensile/Compressive Response of Magnesium Alloy AZ31 by Integrating with Al_2O_3 Nanoparticles, *Mater. Sci. Eng., A*, 2009, **527**, p 162–168
12. M. Paramsothy, J. Chan, R. Kwok, and M. Gupta, The Synergistic Ability of Al_2O_3 Nanoparticles to Enhance Mechanical Response of Hybrid Alloy AZ31/AZ91, *J. Alloys Compd.*, 2011, **509**, p 7572–7578
13. M. Paramsothy, J. Chan, R. Kwok, and M. Gupta, Enhanced Mechanical Response of Hybrid Alloy AZ31/AZ91 Based on the Addition of Si3N4 Nanoparticles, *Mater. Sci. Eng., A*, 2011, **528**, p 6545–6551
14. N. Chawla and Yu-Lin Shen, Mechanical Behavior of Particle Reinforced Metal Matrix Composites, *Adv. Eng. Mater.*, 2001, **3**(6), p 357–370
15. J. Llorca, Fatigue of Particle- and Whisker-Reinforced Metal-Matrix Composites, *Prog. Mater. Sci.*, 2002, **47**, p 283–353
16. T.S. Srivatsan, M. Al-Hajri, and P.C. Lam, The Quasi-Static, Cyclic Fatigue and Final Fracture Behavior of a Magnesium Alloy Metal-Matrix Composite, *Composites Part B*, 2005, **36**, p 209–222
17. A.R. Vaidya and J.J. Lewandowski, Effects of SiCp Size and Volume Fraction on the High Cycle Fatigue Behavior of AZ91D Magnesium Alloy Composites, *Mater. Sci. Eng., A*, 1996, **220**, p 85–92

18. N. Llorca, A. Boyce, and T.M. Yue, Fatigue Behavior of Short Alumina Fiber Reinforced AZ91 Magnesium Alloy Metal Matrix Composite, *Mater. Sci. Eng., A*, 1991, **135**, p 247–252
19. Y. Ochi, K. Masaki, T. Matsumura, and M. Wadasako, Effects of Volume Fraction of Alumina Short Fibers on High Cycle Fatigue Properties of Al and Mg Alloy Composites, *Mater. Sci. Eng., A*, 2007, **468–470**, p 230–236
20. W. Riehemann, Z. Trojanová, and A. Mielczarek, Fatigue in Magnesium Alloy AZ91-γAlumina Fiber Composite Studied by Internal Friction Measurements, *Proc. Eng.*, 2010, **2**(1), p 2151–2160
21. L.M. Tham, M. Gupta, and L. Cheng, Influence of Processing Parameters During Disintegrated Melt Deposition Processing on Near Net Shape Synthesis of Aluminum Based Metal Matrix Composites, *Mater. Sci. Technol.*, 1999, **15**, p 1139–1146
22. M. Gupta, M.O. Lai, and S.C. Lim, Regarding the Processing Associated Microstructure and Mechanical Properties Improvement of an Al-4.5 Cu Alloy, *J. Alloys Compd.*, 1997, **260**, p 250–255
23. M. Gupta and T.S. Srivatsan, Microstructure and Grain Growth Behavior of an Aluminum Alloy Metal Matrix Composite Processed by Disintegrated Melt Deposition, *J. Mater. Eng. Perform.*, 1999, **8**(4), p 473–478
24. P.S. Ling, M. Gupta, M.O. Lai, and T.S. Srivatsan, Recycling an Aluminum Matrix Composite Using the Technique of Disintegrated Melt Deposition, *Alum. Trans.: Int. J.*, 2000, **2**(2), p 209–215
25. V.V. Ganesh, M. Gupta, and T.S. Srivatsan, Disintegrated Melt Deposition Technique: A Near Net Shape Manufacturing Process for Metal-Based Materials, *J. Recent Res. Dev. Mater. Sci. Eng.*, 2002, p 119–136, ISBN: 81-7895-057-X
26. X. Fan, W. Tang, S. Zhang, D. LI, and Y. Peng, Effects of Dynamic Recrystallization in Extruded and Compressed AZ31 Magnesium Alloy, *Acta Metall. Sin.*, 2010, **23**(5), p 334–342
27. Y. Radi and R. Mahmudi, Effect of Al_2O_3 Nano-particles on the Microstructural Stability of AZ31Mg Alloy After Equal Channel Angular Pressing, *Mater. Sci. Eng., A*, 2010, **527**, p 2764–2771
28. Z. Hong-Liang, G. Shao-kang, Z. Fei-yan, L. Qing-kui, and W. Li-guo, Microstructure and Properties of AZ31 Magnesium Alloy with Rapid Solidification, *Trans. Nonferr. Met. Soc. China*, 2005, **15**, p 144–148
29. F. Czerwinski, K.N. Braszczyńska-Malik, Ed., *Magnesium Alloys—Design, Processing and Properties*, InTech, 2011, p 95–112
30. M.S. Yong and A.J. Clegg, Evaluation of Squeeze Cast Magnesium Alloy and Composite, *Foundryman*, 1999, **92**(3), p 71–75
31. S.F. Hassan and M. Gupta, Effect of Particulate Size of Al_2O_3 Reinforcement on Microstructure and Mechanical Behavior of Solidification Processed Elemental Mg, *J. Alloys Compd.*, 2006, **419**(1–2), p 84–90
32. E.D. Francis, N.E. Prasad, C. Ratnam, P.S. Kumar, and V.V. Kumar, Synthesis of Nano Alumina Reinforced Magnesium-Alloy Composites, *Int. J. Adv. Sci. Technol.*, 2011, **27**, p 35–44
33. K.K. Deng, K. Wu, Y.W. Wu, K.B. Nie, and M.Y. Zheng, Effect of Submicron Size SiC Particulates on Microstructure and Mechanical Properties of AZ91 Magnesium Matrix Composites, *J. Alloys Compd.*, 2010, **504**, p 542–547
34. M. Jayamathy, S.V. Kailas, K. Kumar, S. Seshan, and T.S. Srivatsan, The Compressive Deformation and Impact Response of a Magnesium Alloy: Influence of Reinforcement, *Mater. Sci. Eng., A*, 2005, **393**, p 27–35
35. X.-F. Gu, W.-Z. Zhang, Z. Min, and Y.E. Fei, Role of Misfit in Precipitation Crystallography in Non-ferrous Metals, *Trans. Nonferr. Met. Soc. China*, 2007, **17**, p s1–s7
36. J.F. Nie, Effects of Precipitate Shape and Orientation on Dispersion Strengthening in Magnesium Alloys, *Scripta Mater.*, 2003, **48**, p 1009–1015
37. B. Chen, D. Lin, Li Jin, X. Zeng, and C. Lu, Equal-Channel Angular Pressing of Magnesium Alloy AZ91 and Its Effects on Microstructure and Mechanical Properties, *Mater. Sci. Eng., A*, 2008, **483–484**, p 113–116
38. V.V. Ganesh and N. Chawla, Effect of Reinforcement-Particle-Orientation Anisotropy on the Tensile and Fatigue Behavior of Metal-Matrix Composites, *Metall. Mater. Trans. A*, 2003, **34A**, p 342-353